



# Influence of Flow-induced Vibration of a D-VAWT With and Without Leading-edge Rod at Various Pitch Angles

C. B. Maheshwaran, E. Karthik Vel, and S. Nadaraja Pillai<sup>†</sup>

*Turbulence & Flow Control Laboratory, School of Mechanical Engineering, SASTRA Deemed to be University, Thanjavur, Tamil Nadu-613401, India*

<sup>†</sup>Corresponding Author Email: [nadarajapillai@mech.sastra.edu](mailto:nadarajapillai@mech.sastra.edu)

## ABSTRACT

Under specific incoming wind speeds, Darrieus- Vertical Axis Wind Turbines (D-VAWT) have been found to display significant amplitude vibrations. Previous studies mainly examined the D-VAWT's aerodynamics, ignoring flow-induced vibration (FIV). A full-scale measurement of the VAWT mast support structure is used to study the impact of the incoming wind speed ( $V$ ) and pitch angle ( $\alpha$ ). The D-VAWT's rotor rotates when the incoming wind encounters its blades, causing vibrations to be transmitted to the turbine's shaft and other supporting elements. As a result, tip speed and pitch angle, which aid in the turbine's rotation, also play a significant role in producing the FIV. Based on the rotation law, the D-VAWT's rotational rate and the enforced Pitch are proportionate to the cylinder displacement. In contrast to the prior report, the vibrations are caused by vortex-induced vibration (V.I.V.) and galloping, which depend on the turbine's pitch angle and tip speed. V.I.V. predominates at high-pitch angles, while galloping is more common at high blade tip speeds and low-pitch angles. Lastly, a leading-edge rod (L.R.) with a 4 mm diameter is fastened to the turbine's blades to suppress V.I.V., which yields a reasonable outcome. Henceforth, this was the first experimental investigation to comprehend the galloping instability and V.I.V. in D-VAWT at various pitch angles and tip speeds.

## Article History

Received October 7, 2024  
Revised February 18, 2025  
Accepted March 3, 2025  
Available online May 5, 2025

## Keywords:

D-VAWT  
Vortex induced vibration (VIV)  
Galloping  
Leading-edge Rod (LR)

## 1. INTRODUCTION

It is normal for any bluff body to experience flow-induced vibrations (FIV) when exposed to wind. This vibration occurs in practically every system now in use, including offshore structures, buildings, towers, trees, airplane wings, and wind turbines. The FIV can produce both helpful motion and nearly severe vibrations. The fluid flow and the elastic forces are interdependent because the fluid forces cause the body to deform, and the fluid forces also change in orientation when the body deforms (Abdelkefi et al., 2012). The most significant system that uses wind energy is the wind turbine, a mechanical device that transforms some of the wind's kinetic energy into valuable electrical energy. Due to its operating independence from wind direction and its low cost of design, installation and maintenance, the straight Darrieus Vertical Axis Wind Turbine (D-VAWT) is widely utilized in the industrial and commercial sectors (Davandeh & Maghrebi, 2023). Understanding fluid-structure coupling is essential to designing wind turbine

systems that meet the requirements better, especially since these wind turbine types are prone to FIV.

A wealth of literature is available for theoretical and analytical research on VAWT. A numerical investigation of the VAWT turbine revealed that the vibrations in the turbine shaft were caused by unstable aerodynamic forces acting on the turbine's blades. The primary cause of the unstable forces in the turbine was the pitch angle of the VAWT (Simão Ferreira et al., 2007). Experimental vibration analysis was done to regulate the shaft's vibration in a small-scale VAWT. According to the study, a shift in pitch angle is once more what causes the vibrations to occur (Castellani et al., 2018). Pitch angle variations generate extremely high aerodynamic loads on the turbine's blades, which are then transferred to the turbine shaft (Bel Mabrouk et al., 2017). The pitch angle variation in the wind turbine determines the upwind and downwind shedding vortices that occur in the structure. According to (Dunne & McKeon, 2015), the shedding vortices cause a strong vibration in the turbine's structure. VAWT, which has a high solidity ratio, often performs

NOMENCLATURE			
D-VAWT	Darrius -Vertical Axis Wind Turbine	$f_n$	natural frequency of d-VAWT
$\alpha$	rotational angle of D-VAWT	$m^*$	mass ratio
V	wind speed	A	oscillating amplitude
$L_R$	leading edge rod	$U^*$	reduced velocity
VIV	vortex-induced vibration	$S_t$	Strouhal number
FIV	flow induced vibration	$C_L$	coefficient of lift
$\rho$	fluid density	$F_v^* = F_v/f_n$	normalised vortex emission frequency
D	diameter of the rotor	$F_{ST}$	vortex emission frequency at rest
d	diameter of the shaft	F	oscillating frequency of d-VAWT
m	mass of the d-VAWT	$F_v$	vortex frequency of d-VAWT
$A^* = A/d$	amplitude ratio	$A^{**}$	non-dimensional acceleration in across wind direction
$t^*$	non dimensional time	$r_l$	constant
y	across wind displacement	c	chord length of the blade
H	height of the blade	$Re_C$	chord based Reynold's number
$Re_D$	diameter based Reynolds number	Fr	Froude's number

well at low tip speeds (Maheshwaran et al., 2023). However, when tip speeds rise, vibrations from the blade are transferred to the supporting structures, resulting in higher structural collapse and reduced reliability (Peng et al., 2019). A computational analysis of the vibrations in a wind turbine gear system revealed that the vibration was more unpredictable around the resonance region of the shaft, which was determined by the turbine's tip speed (Wei et al., 2015). According to (Nguyen et al., 2021), a computational and experimental investigation also confirms the vibration in VAWT at a low tip speed ratio, which may be caused by wake creation in the downwind region. According to a study, the incoming wind speed significantly impacts the turbine's vibrations (Hamdi et al., 2014). Large-scale vortex formations in the turbine were caused by low blade speed ratios (0.4 to 2.3) and high solidity ratios (McLaren et al., 2012). The research as mentioned above supports the anomalous vibrations observed in VAWT, and the pitch angle and tip speed are the main factors influencing these vibrations. However, no documented experimental investigations have been made as of yet. It is commonly known that flow-induced vibrations (FIV) can cause significant amplitude vibrations in elastic bodies. If these vibrations are not adequately reduced, they may lead to excessive stress (Zuo & Letchford, 2010). When the shedding frequencies of vortices coincide with the natural frequency of the structure, a kind of FIV known as Vortex-Induced Vibration (V.I.V.) occurs in the opposite direction of the wind (Piersol & Paez, 2010). The intricate interplay between the wind turbine and fluid flow is contingent upon numerous fluid flow-related parameters, including Reynolds number, structural attributes (mass, stiffness, and damping coefficients), and body geometry. A D-VAWT functions as a rigid circular cylinder driven by a uniform fluid flow, so V.I.V. is highly relevant to wind turbines. Therefore, the primary focus has been determining how the turbine's pitch angle and incoming wind speed affect the V.I.V. response. With the presence of various passive flow control devices such as a Leading Edge Prism Shaped Cylinder (Fatahian et al., 2024), a 20 % decrease in the radius of the leading edge of the VAWT blade (Davandeh & Maghrebi, 2023) have notably improved the performance of the VAWT. However, the

presence of LEP has decreased the vibration when compared to the straight blade VAWT (Karthik Vel & Nadaraja Pillai, 2024). It has a better self-starting capability (Elangovan & Pillai, 2025). Further, with the help of introducing the leading edge rod, there is a relative increment of 210.9% of tangential force and 42.1% of power coefficient for 2blade D-VAWT, thus the vortices shed from the leading edge rod has drastically reduced the formation of dynamic stall vortices (Zhong et al., 2019).

Galloping is the other kind of issue that arises in the FIV. Galloping is another example of an across-wind oscillation that occurs when an object revolves at high speeds. Unlike V.I.V., it doesn't depend on lock-in zones and is primarily driven by the immediate angle of attack between the body and the incoming flow (Kaczinski et al., 1998). Because D-VAWT is a type of bluff body in varying pitch angle and incoming wind speed conditions, there are many reasons for galloping instability. Numerous investigations were conducted to comprehend the flow mechanics surrounding the circular cylinder. Thrust was produced by translational and rotational oscillations (Blackburn et al., 1999). Following this investigation, (Nazarinia et al., 2009a, b) found new wake modes surrounding the circular cylinder, where translational and rotational oscillation produces thrust. Similarly, phase shift may be used to lessen the synchronization zone of cylinder motion in the near wake, according to (Al-Mdallal, 2004) and (Nazarinia et al., 2009b). In the preceding research, the rotation placed on the cylinder is unrelated to the cylinder's dynamics and, hence, uncoupled from the outcome of the Fluid-Structure interaction. (Lu et al., 2011) advanced in this sense by rotating a fixed circular cylinder with a time-dependent angular speed proportional to the fluctuating lift coefficient to reduce lift force. (Vicente-Ludlam et al., 2017) investigated how the rotation of a cylinder is proportional to the position of the cylinder.

In this study, the wind turbine (D-VAWT) is assumed to be a rigid circular cylinder, with the rotation of the wind turbine being proportional to the blade's position. If  $\alpha$  is the blade's rotation angle, then ( $\alpha = r_l y$ ), where y is the D-

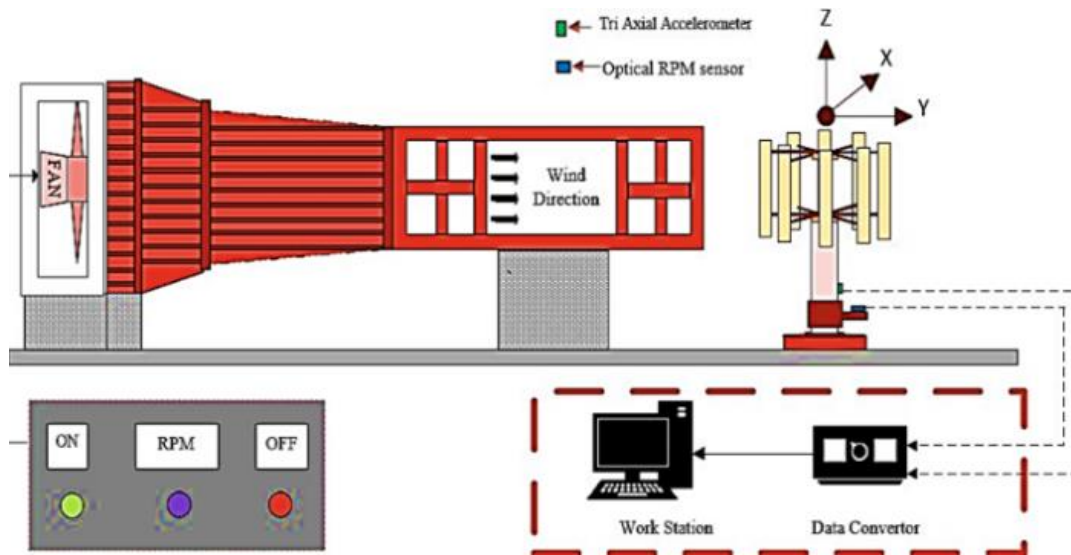


**Fig. 1** Experimental setup includes a vertical axis wind turbine (VAWT) and an axial blower. The accelerometer is mounted to the shaft

VAWT rotor shaft displacement and  $r_1$  is constant. It is widely known that oscillations in the blades will be conveyed to the turbine's shaft, which serves as the supporting system. Thus, the rotary motion imposed by the blade is proportional to the displacement of the D-VAWT shaft. The experimental acceleration data has been obtained and illustrated by changing the pitch angle and tip speed of the D-VAWT.

## 2. EXPERIMENTAL METHODOLOGY

### 2.1 Formulation

A Darrieus VAWT with 8 blades was built, with the blade profile being S1046. The chord value of the blade is taken as 0.14m, the turbine's total height is 1.5m, and the rotor diameter is 0.9m. The blade height (blade span) is 0.7m to evaluate the adverse effects of vibrations on the turbine. The rotor has relatively high solidity  $Nc/\pi D = 0.39$  and low aspect ratio  $(H/D) = 0.78$  generally taken for D-VAWT (Miller et al., 2018). To validate the operation of the D-VAWT, nondimensional VAWT parameters such as Reynolds number, and Froude's number were explored in accordance with previous research. (Ross & Polagye, 2022). The incoming wind speed range was chosen to be from 4 and 24 meters per second, and the air temperature is approximately 28 °C. The chord-based Reynolds number ( $Re_c$ ) ranges from  $35,800 \leq Re \leq 2,14,800$ , while the diameter-based Reynolds number ( $Re_D$ ) is  $2,30,400 \leq Re \leq 1,382,400$ . In this study, the chord-based Reynolds number ranges from 104~105, while the diameter-based Reynolds number ranges from 105~106. This places the turbine in a Reynolds number-independent region, allowing for reasonable performance in full scale studies (Bachant & Wosnik, 2016). The Froude's number is calculated based on the formula  $Fr = V/(g \times l)$  where  $l$  is said the channel depth. The number is found to be  $1.04 \leq Fr \leq 6.23$ .

In this experiment, the symmetrical S1046 blade profile was used because it was found to increase the efficiency of VAWT (Mohamed, 2012). The fluctuation in

pitch angle was within  $\pm 30^\circ$ . This was made possible by using the VAWT's adjustable blade pitch angle design. Each blade's angle can be adjusted every  $3^\circ$ . Since FIV has a larger impact on VAWT in this region, blade angles were changed from  $0^\circ$  to  $21^\circ$  in this experiment (McLaren et al., 2012). In addition to the standard blades, the S1046 Blades are fastened to the leading-edge rod (LR) to regulate the FIV vibrations. The diameter of the rod, 4mm, was determined to be the ideal choice for the optimal location of the LR, and it is positioned precisely 4cm from the trailing edge.

The axial wind blower facility in SASTRA, which is the University's Aerodynamics lab, provided the experimental data that was extracted for this study. As seen in Fig.1, a control panel can be used to operate the fan that drives the axial wind blower (Maheshwaran et al., 2023). The wind tunnel's test section can reach a maximum wind speed of 28 m/s. Prior to experimentation, the wind velocity for the different rotational speeds in this study was calibrated. A triaxial accelerometer was used to continually monitor the VAWT system's dynamic response. A data collecting system continually sampled the accelerator coupled to the turbine shaft at a sampling frequency rate of 2560 Hz. For 16s, data was continually collected. An eight-bladed high solid VAWT was used for the aforementioned investigation. As shown in Fig. 2.a, the accelerometer was positioned at position 1. However, the accelerometer was positioned at four different positions in order to comprehend the dynamics of the VAWT. As illustrated in Fig. 2.b, the accelerometer data acquired at position 1 were only taken for the blade positions from  $\alpha = 0^\circ$  to  $45^\circ$ . Readings between  $0^\circ$  and  $45^\circ$  were taken while the blade rotated. After accurately converting the recorded accelerometer value to displacement, the data was examined. A coordinate system similar to the one in the illustration was utilized to comprehend the vibrational property. The along wind directions are represented by the y-direction in the coordination system and the across wind directions by the x-direction. The shaft or the rotor shaft rotation speed was

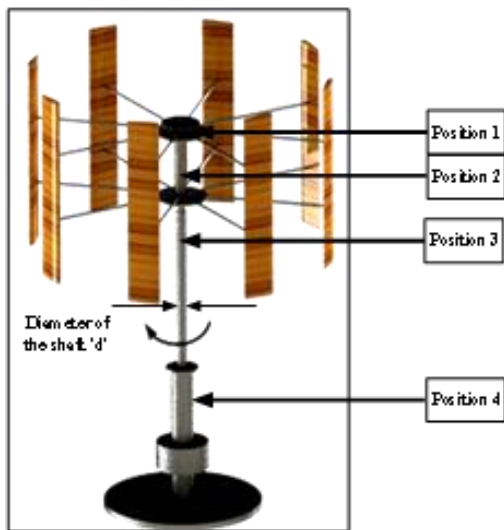


Fig. 2a Demonstrates the accelerometer's position and an eight-bladed VAWT

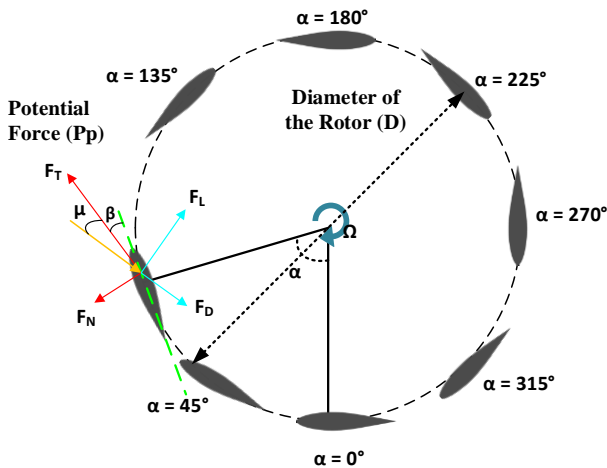


Fig. 2b Schematic view of the acceleration monitored VAWT (top view)

measured using an optical type RPM measurement equipment that converts mechanical motion to an electric pulse. Only the across-wind response is shown since there was a slight change in the response seen in the along-wind response.

### 2.2 Modal Analysis for Vertical Axis Wind Turbine

Initially, a preliminary modal analysis was undertaken to identify the natural frequency of the VAWT structure. This investigation sought to understand the wind load excitations resulting from modifications in the aerodynamics of straight blades.

The frequency at which the structure was excited was determined by placing a triaxial accelerometer at position 1 and subjecting it to random load excitations at different locations, as illustrated in Fig. 2a. The wind induced vibration generally occurs in the low frequency region, hence the position 1 was taken for the study. Subsequently, the structural responses were analyzed, resulting in the identification of three distinct frequencies were listed in the Table 1 with magnitudes of 11.23 Hz,

Table 1 Natural frequency of the D-VAWT at various position

Position	Mode 1 (Hz)	Mode 2 (Hz)	Mode 3 (Hz)
Position 1	11.25	58.1	101.8
Position 2		58.1	101.8
Position 3		58.1	101.8
Position 4			101.8

58.11 Hz, and 101.8 Hz. The study's main findings indicate that position 4 was shown to be vibrant with the highest point at 101.8 Hz, and position 3 also exhibited a peak at the same frequency.

The study found that position 1 had a low-frequency peak at 11.23 Hz, while position 2 had a peak at 58.11 Hz. The research provided the three natural frequencies that were excited by the structure, as shown in Fig. 3., which helps to understand the shift in the frequency response of the VAWT as it operates at different wind speeds.

The rotation of VAWT ( $\alpha$ ) around its own axis is enforced. The shaft displacement  $y$  is proportional to the VAWT rotation ( $\alpha$ ) around its own axis. The differential equation for the VAWT system is derived from the balance of inertia, fluid forces, and stiffness.

$$m\ddot{y} + ky = \frac{1}{2}\rho_a V^2 D C_L \tag{1}$$

Where  $y$  represents the across wind displacement of the shaft,  $\rho_a$  is the fluid density,  $V$  is the free stream velocity,  $D$  is the rotor's diameter, and  $C_L$  is the fluid force coefficient in the across direction to the incoming flow. The rotation of the shaft has been assumed to be proportional to the displacement.

$$\alpha = r_1 y \tag{2}$$

Where  $r_1$  is a constant.

Introducing the non-dimensional variables,

$$A^* = A/d; \text{ and } t^* = f_n t; \text{ where } f_n = \frac{\sqrt{k/m}}{2\pi}.$$

From this, equation 1 becomes,

$$A^{*''} + 4\pi^2 A^* = \frac{2U^{*2} C_L}{\pi m^*} \tag{3}$$

Where  $m^* = \frac{4m}{\pi \rho_a d^2}$  is the mass ratio;  $U^* = V/f_n d$  is called the reduced velocity;  $d$  shaft diameter.  $A$ - oscillating amplitude of D-VAWT shaft

## 3. RESULTS AND DISCUSSION

### 3.1 Wind Turbine Rotor Dynamics for 0° Pitch angle

The wind turbine rotor oscillates in a periodic manner that is nearly entirely sinusoidal. For all values  $A^* = A/d$  of the rotor's steady state oscillations, oscillations revolve around an equilibrium point because of the imposed rotation's character, which prevents symmetry from being broken (Govardhan & Williamson, 2006) discovered that the VIV curve for the Reynolds number over  $Re = 600$  consisted of three branches: the first upper branch, a lower branch, and a third branch that dealt with the amplitude

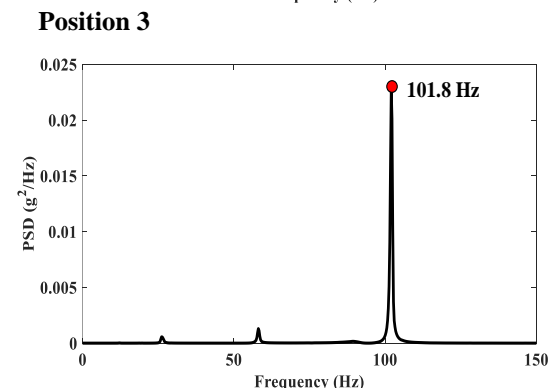
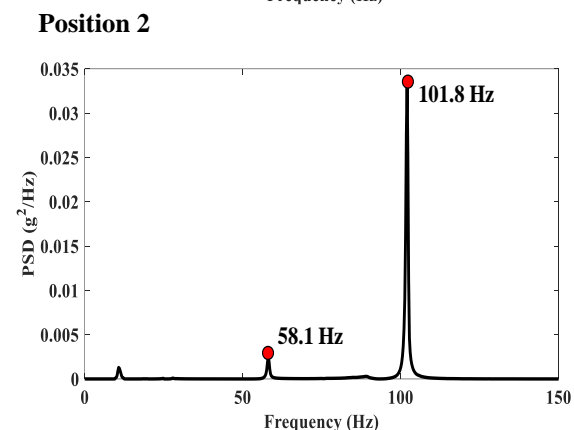
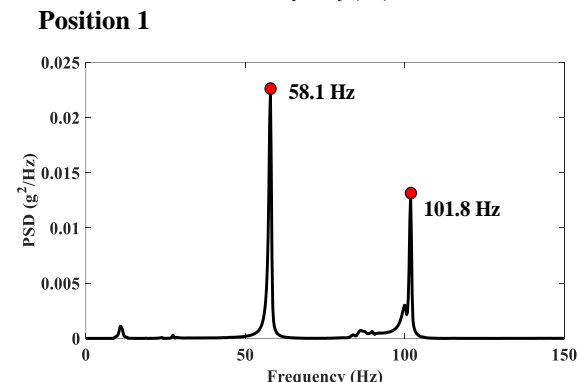
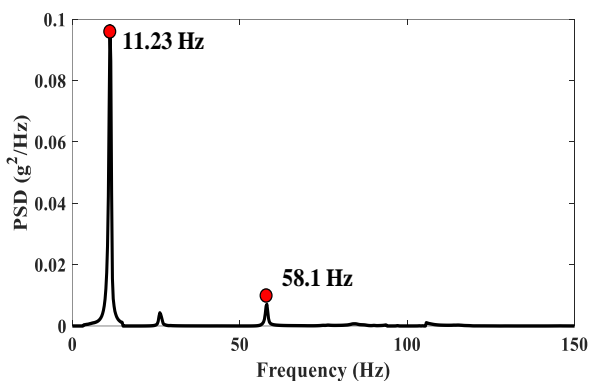


**Fig. 3 Frequency spectra of the structural response for different modal excitation**

response for a cylindrical body. The upper branch is absent for lower Reynolds numbers. The relationship between  $U^*$  and  $A^*$  and the mean displacement plot for pitch angle  $0^\circ$  are shown in Fig. 5.

As it can be seen from Fig.5, the transition from the initial up to lower branch is absent here, where no

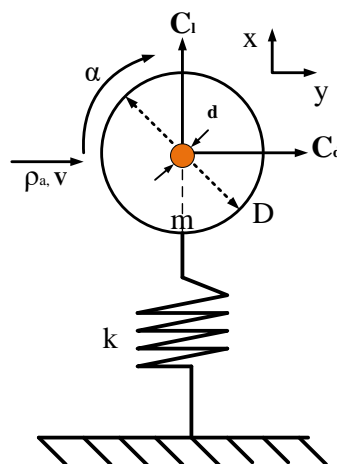


**Fig. 4 Schematics of the rotating VAWT**

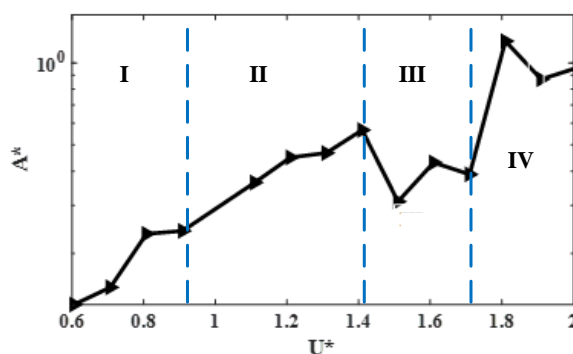


**Fig. 5 Logarithmic non-dimensional amplitude oscillations as a function of the reduced velocity for the pitch angle  $0^\circ$**

synchronization region is present. The region I, II, III, and IV show a quasi-linear dependence between  $A^*$  and the reduced velocity  $U^*$ . This implies there is no synchronization region and confirms the absence of VIV. As a result, these fluid force types typically resemble the motion-induced, galloping kind of instability. For pitch angle  $0^\circ$ , the normalized frequency of oscillations,  $f^*$ , is presented as a function of reduced velocity in Fig 6 Additionally, a bold solid line ( $F_{st} = \frac{StD}{U}$ ) that displays the vortex emission at rest compares the Strouhal law. The other line ( $F_v^* = f_v/f_N$ ) depicts the vortex emission while the rotor is in motion. The Fig.6 represents the PSD of the oscillating frequency and vortex frequency. The relation with  $F^*$  and  $F_v^*$  says the synchronization region in a particular frequency spectrum, if  $F^*$  and  $F_v^*$  are closer to each other, it is well known that the region has been synchronized and there is an increase in oscillations. Hence, when these two terms are within close range, the amplitude rise signifies the VIV. If  $F_v^*$  and  $F^*$  are not close but still there is an increase in amplitude, this is evidence of flow-induced vibration or it can be simply said as galloping instability of a structure.

From Fig.6. the initial oscillating frequency  $F^*$  is well below the value of '1', and when the reducing velocity increases, the frequency value increases up to 1 and remains almost constant in that region. For  $U^* = 0.8$  and

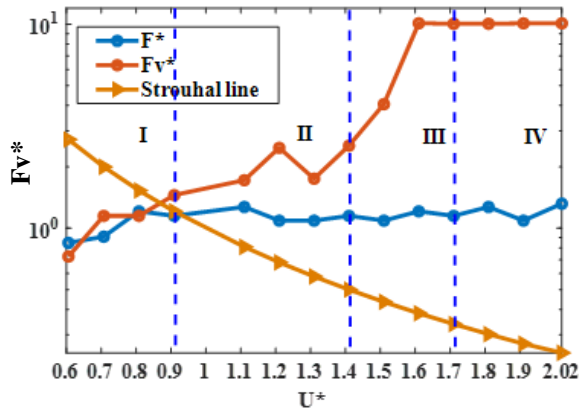


**Fig. 6**  $F^*$  Normalized oscillation frequency;  $F_v^*$  Normalized vortex emission frequency; Strouhal Line as a function of decreased velocity for the value =  $0^\circ$ - $45^\circ$  at pitch angle  $0^\circ$

0.9, the oscillating frequency  $F^*$  is in close range with the Strouhal line at rest. This can probably induce VIV in this region. But the vortex frequency spectrum  $F_v^*$  almost continuously increases from the initial value, which shows the non-dependence with  $F^*$ . The region I in Fig.6, where  $U^* = 0.8$  and  $0.9$ , seems to be a lock in the regions of  $F^*$  and  $F_v^*$ , which cannot be confirmed as VIV because when the  $U^*$  reaches a higher value, there is no dependence on the vortex frequency. Hence, it is evident that the flow-induced vibration is due to the galloping of the rotor system and is completely independent of VIV. As it can be seen in Fig.6, in regions II, III, and IV ( $0.9 < U^* < 2.02$ ), the oscillating frequency  $F^*$  is markedly diverging from the vortex frequency  $F_v^*$ , which is again proof of negative oscillations happening in the wind turbine rotor system.

### 3.2 Wind Turbine Rotor Dynamics for $3^\circ$ Pitch Angle

Wind turbine rotors vibrate significantly at  $0^\circ$  pitch angle, consistent with prior results. Similar to the previous study, flow-induced vibrations will be classified as VIV or galloping based on the relationship between reduced velocity ( $U^*$ ), mean displacement ( $A^*$ ), oscillation frequency ( $F^*$ ), and vortex frequency ( $F_v^*$ ).

Figure 7 illustrates the relationship between reduced velocity ( $U^*$ ) and mean displacement ( $A^*$ ). From the figure, it is clear that the relationship is not linear, as in the case of the  $0^\circ$  pitch angle. The amplitude in the region I initially increases and remains constant for a period of  $0.6 < U^* < 1.01$ . For the region II ( $U^* = 1.1$  and  $1.2$ ), the value decreased considerably and started to increase in regions III and IV ( $U^* = 1.3$  to  $2.02$ ). The turbine rotor system experiences an increase and decrease in amplitude in regions I and II, which denotes the flow-induced vibration, which could be VIV ( $0.6 < U^* < 1.2$ ). In regions III and IV, the amplitude varies almost linearly, similar to the case of  $0^\circ$  pitch angle (quasi-linear), which could be a confirmation of galloping instability induced by the increasing speed of the turbine rotor. Hence, both vortex-induced vibration and galloping vibrations could possibly occur at pitch angle  $3^\circ$ , which is confirmed by analysing the frequency spectrum.

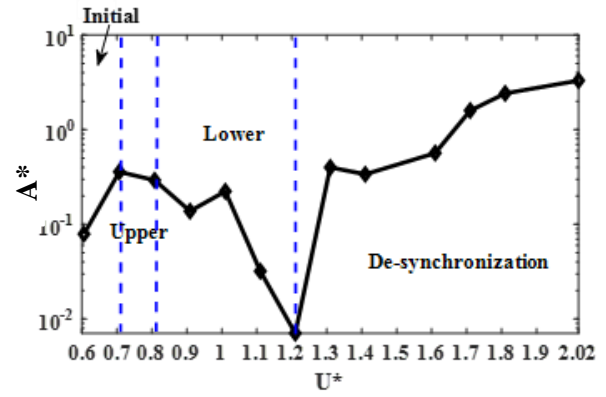


**Fig.7** Logarithmic non-dimensional amplitude oscillations as a function of the reduced velocity for the pitch angle  $3^\circ$

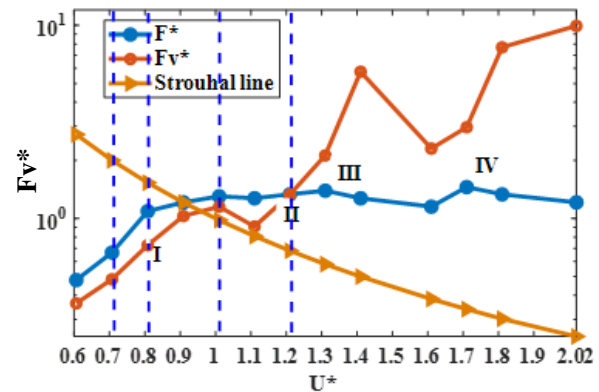


**Fig. 8**  $F^*$  Normalized oscillation frequency;  $F_v^*$  Normalized vortex emission frequency; Strouhal Line as a function of decreased velocity for the value =  $0^\circ$ - $45^\circ$  at pitch angle  $3^\circ$

From Fig.8, the initial excitation frequency at the region I ( $U^*=0.6$ ) drops dramatically from its natural frequency value of '1'. As  $U^*$  increases, so does  $F^*$ , until it reaches a value closer to '1', at which point it remains constant ( $U^*=0.8$ ) while the rotor oscillates considerably. At  $U^*=1.2$ , the synchronization region between the vortex shedding ( $F_v^*$ ) and oscillating frequency ( $F^*$ ) ends, at which the value of  $A^*$  practically is '0'. The region II ( $0.9 < U^* < 1.2$ ) the value of  $F^*$  and  $F_v^*$  are almost closer to the Strouhal line, which is the vortex emission frequency at rest. This result is similar to that of (Govardhan-&Williamson, 2006) study where the vortex shedding component has a  $180^\circ$  phase change with oscillating frequency. For this reason, it is confirmed that the oscillation taking place in the rotor system is found to be VIV in between the region  $0.6 < U^* < 1.2$ . Further from the region III and IV ( $1.3 < U^* < 2.02$ ) the maximum amplitude ( $A^*$ ) value reaches closer to '3' and  $F_v^*$  value increases linearly. From  $U^*=1.3$  to  $2.02$  the  $F_v^*$  is independent which deviates more from  $F^*$  which confirms there is no synchronisation between the frequencies. Clearly the regions III and IV experience negative oscillations which confirms the presence of galloping.

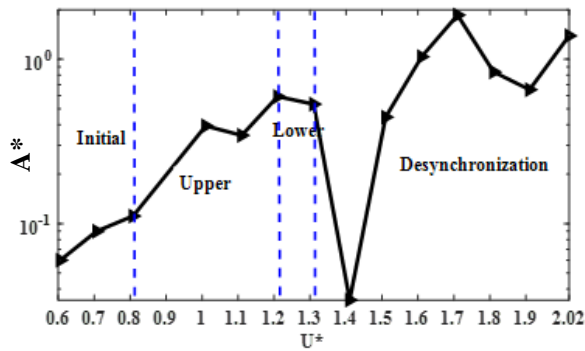


**Fig. 9** Logarithmic Non-dimensional amplitude oscillations as a function of the reduced velocity for the pitch angle  $6^\circ$

### 3.3 Wind Turbine Rotor Dynamics for $6^\circ$ Pitch Angle

From the Fig. 9, the amplitude rise is not linear as in the case of  $0^\circ$  pitch angle but it looks similar to  $3^\circ$  pitch. Unlike the amplitude in region I, that grows immediately for pitch angle  $3^\circ$ , it increases here slowly and attains the peak at  $U^*=1.2$  with the maximum value of  $A/d=0.6$ . The value declined significantly in region II ( $U^* = 1.4$ ) before gradually increasing in regions III and IV ( $U^* = 1.5$  to 2.02).

Similar to the previous case, the turbine rotor system undergoes an increase and drop in amplitude in areas I and II, indicating flow-induced vibration, which could be VIV ( $0.6 < U^* < 1.4$ ). In regions III and IV, the amplitude varies approximately linearly, analogous to the situation of  $0^\circ$  pitch angle (quasi-linear), indicating galloping instability caused by the turbine rotor's growing speed. Analysis confirms that both vortex-induced and galloping vibrations may arise at pitch angle of  $6^\circ$ . Another significance of this pitch angle is that the initial excitation happens only at  $U^* = 1.2$ , whereas the peak occurs at  $U^* = 0.7$  at the  $3^\circ$  pitch angle. Also, the lock-in region is remarkably increased from  $U^*=1.2$  to 1.4, which indicates the formation of different forms of wake at pitch angles  $3^\circ$  and  $6^\circ$ . Further investigation is required to understand the dynamics of the wake pattern.

As it can be seen from the Fig.10, the oscillating frequency initially increases and remains fairly constant in the region I and II. Also, at  $U^*=1.4$  the synchronization region ends and the two frequency spectrums separate from each other. This again resembles the case of pitch angle  $3^\circ$  where the VIV is responsible for the induction of amplitude in the rotor system. The vortex frequency line in the range  $0.9 < U^* < 1.2$  lies closer to the Strouhal line which would probably excite VIV in the system as per (Singh & Mittal, 2005). Further, as the  $U^*$  increases ( $1.5 < U^* < 2.02$ ) the  $F_v^*$  grows and it is completely deviated from the oscillating spectrum  $F^*$ .

This shows that the amplitude rise is purely based on the rotational speed of the rotor rather because of the lock in region. Hence at high rotational speed, the turbine rotor is susceptible to galloping type of vibrations rather than the VIV.

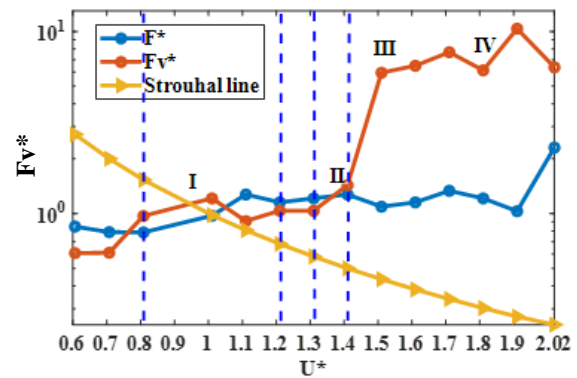


**Fig. 10**  $F^*$  Normalized oscillation frequency;  $F_v^*$  Normalized vortex emission frequency; Strouhal Line as a function of decreased velocity for the value =  $0^\circ$ - $45^\circ$  at pitch angle  $6^\circ$

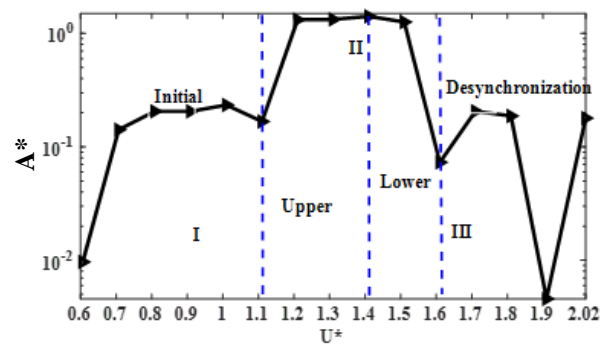


**Fig. 11a** Logarithmic Non-dimensional amplitude oscillations as a function of the reduced velocity for the pitch angle  $9^\circ$

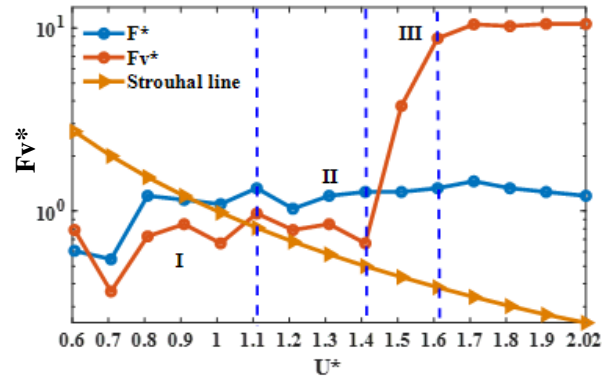


**Fig. 11b**  $F^*$  Normalized oscillation frequency;  $F_v^*$  Normalized vortex emission frequency; Strouhal Line as a function of decreased velocity for the value =  $0$ - $45^\circ$  at pitch angle  $9^\circ$

### 3.4 Wind Turbine Rotor Dynamics for $9^\circ$ Pitch Angle

The Fig. 11a, shows that the transition from the initial excitation is delayed until  $U^*=1.1$ , with a maximum amplitude of  $A^*=1.3$ . In addition, the lock-in period has been greatly extended. According to Fig. 11a and b., when  $U^*=1.5$ , desynchronization between the rotor's oscillating

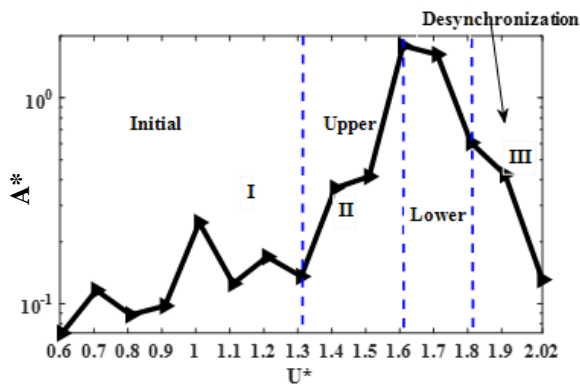


**Fig. 12a** Logarithmic Non-dimensional amplitude oscillations as a function of the reduced velocity for the pitch angle  $12^\circ$

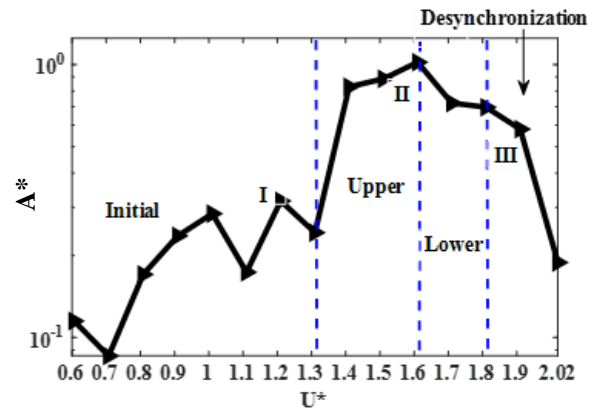


**Fig. 13a** Logarithmic Non-dimensional amplitude oscillations as a function of the reduced velocity for the pitch angle  $15^\circ$

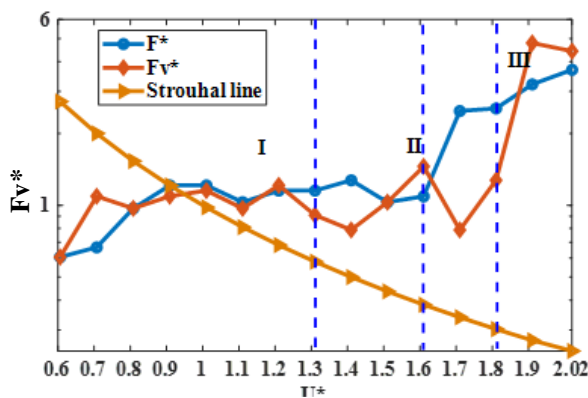


**Fig. 12b**  $F^*$  Normalized oscillation frequency;  $F_v^*$  Normalized vortex emission frequency; Strouhal Line as a function of decreased velocity for the value =  $0^\circ$ - $45^\circ$  at pitch angle  $12^\circ$

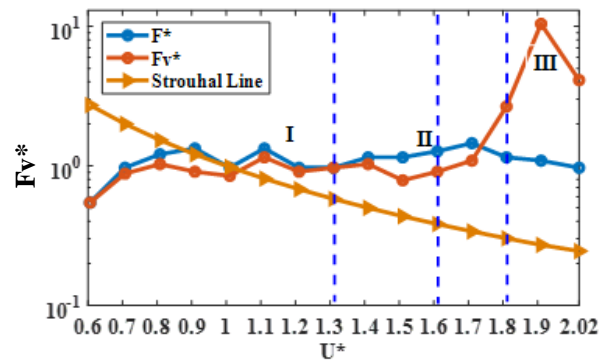


**Fig. 13b**  $F^*$  Normalized oscillation frequency;  $F_v^*$  Normalized vortex emission frequency; Strouhal Line as a function of decreased velocity for the value =  $0^\circ$ - $45^\circ$  at pitch angle  $15^\circ$

frequency and the vortex emission frequency occurs, resulting in a decrease in the amplitude of oscillation. The enormous amplitudes of vibration also occur for  $F^* \approx F_v^* \approx 1$ , except at particular locations like  $U^* = 1.5$ , when the dominant frequency  $F_v^*$  deviates from  $F^*$ . According to (Vicente-Ludlam et al., 2018) these forms of oscillations are mostly driven by VIV type, and the circulation of the vortices being shed becomes stronger. When comparing Fig.7, it is obvious that the amplitude is high for  $U^* = 1.5$  and  $1.6$ , but desynchronization begins at the specified velocity. This is caused by the D-VAWT rotating in the same direction as the vortices being shed, while vortex emission and cylinder oscillations (till  $U^* = 1.4$ ) are synchronized. As the circulation of these vortices increases, so does the amplitude of the vibration.

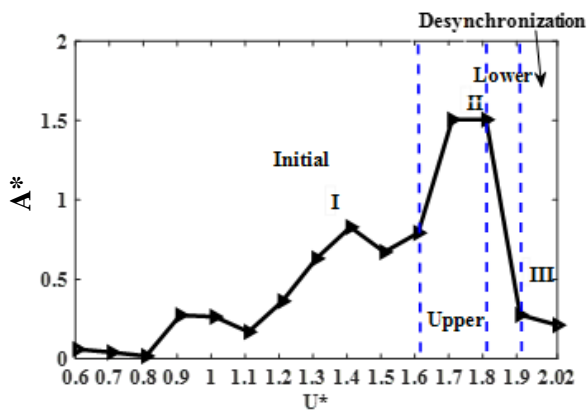
### 3.5 Wind Turbine Rotor Dynamics for $12^\circ$ Pitch Angle

Figure 12a illustrates the change of  $A^*$  with  $U^*$ , whereas Fig.11b, displays the behavior of  $F_v^*$  and  $F^*$  at pitch angle  $12^\circ$ . The figure illustrates how the first excitation is significantly delayed up to region I, where  $0.6 < U^* < 1.3$ . (Govardhan et al., 2000) states that although the  $F_v^*$  and  $F^*$  have a lock-in point, the shedding vortices may be pointing in the opposite direction of the rotating

rotor, which could suppress the amplitude in this area. The amplitude rise and lock-in region are important in area II ( $U^* = 1.5 - 1.7$ ). The fall in amplitude in Region III can be attributed to a phase difference between the oscillation frequency and the vortex frequency, just like in Region I. This indicates that the turbine experiences VIV at a pitch angle of  $12^\circ$  during the duration, and the amplitude rise is realized in the region ( $U^* = 1.5$  to  $1.7$ ). It is noteworthy that although the turbine's rotation speed increases, the amplitude does not. This indicates that there is no galloping wind-induced vibration at the relevant pitch angle.

### 3.6 Wind Turbine Rotor Dynamics for $15^\circ$ Pitch Angle

As seen in Fig.13a, the transition from the initial excitation to the lower branch ( $U^* = 0.6$  to  $1.3$ ) region I is delayed until  $U^* = 1.3$ , resembling the pitch angle  $9^\circ$  in this instance. Likewise in the case of pitch angle  $9^\circ$ , two branches gradually descend to the lower region as they switch from the lower to the upper branch. The VIV is the cause behind this. Figure 13b, provides additional confirmation of this, showing that the  $F_v^*$  and  $F^*$  region exhibits a significant synchronization zone up to  $U^* = 1.7$ . The vortex spectrum splits off from the oscillating spectrum precisely at this region II ( $U^* = 1.8$ ), marking the



**Fig. 14a** Logarithmic Non-dimensional amplitude oscillations as a function of the reduced velocity for the pitch angle 18°

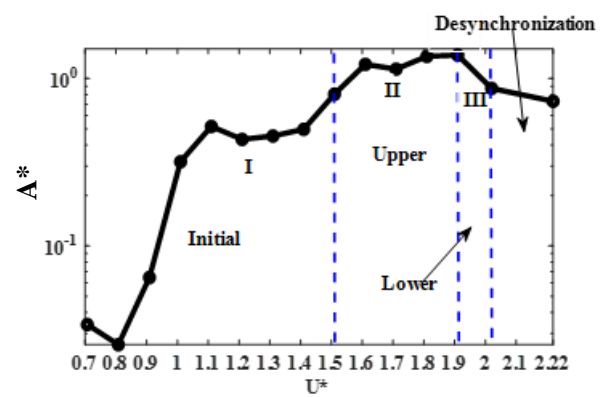


**Fig. 15a** Logarithmic Non-dimensional amplitude oscillations as a function of the reduced velocity for the pitch angle 21°

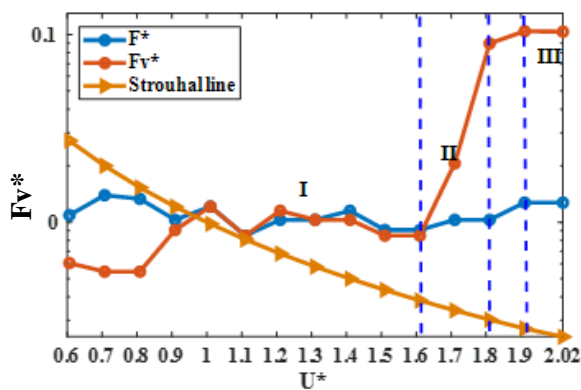


**Fig. 14b**  $F^*$  Normalized oscillation frequency;  $F_v^*$  Normalized vortex emission frequency; Strouhal Line as a function of decreased velocity for the value = 0°-45° at pitch angle 18°

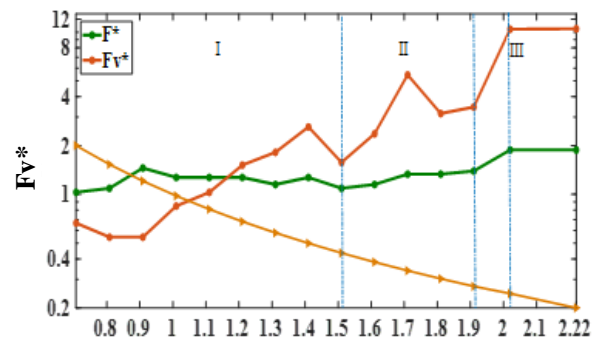


**Fig. 15b**  $F^*$  Normalized oscillation frequency;  $F_v^*$  Normalized vortex emission frequency; Strouhal Line as a function of decreased velocity for the value = 0°-45° at pitch angle 21°

conclusion of the lock-in region.  $A^*$  periodically declines and there is a distinct divergence with a vortex spectrum at area III ( $U^*=1.9$  and  $2.02$ ). Consequently, galloping doesn't occur here, and the vibration that is caused is again due to VIV.

### 3.7 Wind Turbine Rotor Dynamics for 18° and 21° Pitch Angle

The non-dimensional amplitude gradually grows as the reduced velocity rises, as illustrated in Fig.14a. The amplitude grows consistently from  $U^*=0.6$  to  $1.4$ , especially in region I. Fig. 13b shows that there is a variance in the oscillating spectrum and vortex spectrum when  $U^*=0.6$  to  $0.8$ , indicating that no VIV is involved. The VIV begins to develop gradually when the  $F_v^*$  matches the  $F^*$ , just like in the earlier pitch angles. The maximum vibration amplitude in region II ( $U^*=1.5$  to  $1.7$ ) occurs at  $A^*=1.6$ . Similar to the VIV type, the amplitude value decreases in region III and fits the lower branch.

As the reduced velocity increases, the non-dimensional amplitude progressively increases, as shown in Fig.15a. From  $U^*=0.6$  to  $1.6$ , the amplitude increases steadily, particularly in region I. When  $U^*=0.6$  to  $0.8$ , Fig.14b demonstrates that there is a variance in the oscillating spectrum and vortex spectrum, suggesting that there is no

involvement of VIV. Just like in the previous pitch angles, the VIV starts to progressively develop when the  $F_v^*$  matches the  $F^*$ . In area II, where  $U^*=1.5$  to  $1.9$ , the highest vibration amplitude happens at  $A^*=1.8$ . The amplitude value fits the bottom branch and drops in region III, much like the VIV type.

### 3.8 D-VAWT with Leading Edge Rod

As shown in Fig. 16, the S1046 blades are fastened to the leading-edge rod (LR) in order to regulate the FIV vibrations. The diameter of the rod 4mm, was determined to be the ideal choice for the optimal location of the LR, and it is positioned precisely 4cm from the trailing edge. The LR is usually placed to suppress the VIV rather than the galloping type of oscillation. By controlling the vortex separation, the LR effectively lessens the turbine's fluctuations at low turbine speed. As explained before, the normal S1046 blade profile exhibits large vortices and a longer synchronization region between the pitch angles 15° to 21°. Hence in this study, two distinct pitch angles 15° and 21° were taken and studied.

### 3.9 Wind Turbine Rotor Dynamics for LR at 15° Pitch Angle

As shown in Fig.17a, the initial transition takes place, and after that,  $A^*=A/d$  exhibits a quasi-linear dependence with  $U^*$ , which resembles the galloping type. Hence, the

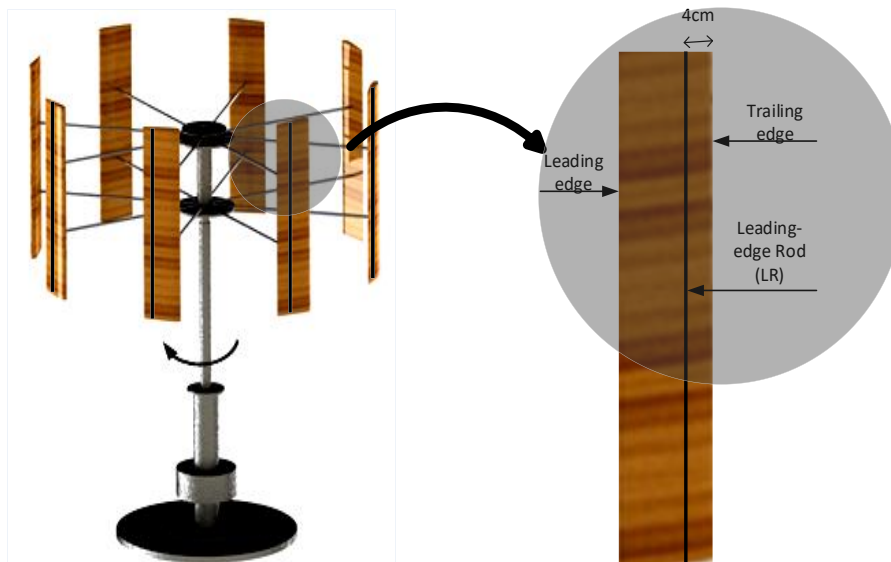


Fig. 16 Placement of leading-edge rod (LR) in the S1046 blade

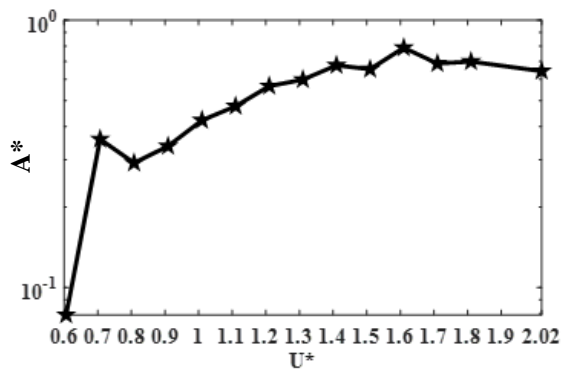


Fig. 17a Logarithmic Non-dimensional amplitude oscillations as a function of the reduced velocity for the pitch angle 15°

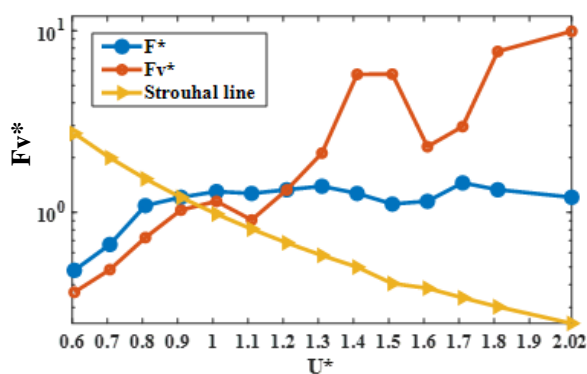


Fig. 17b  $F^*$  Normalized oscillation frequency;  $F_v^*$  Normalized vortex emission frequency; Strouhal Line as a function of decreased velocity for the value = 0-45° at pitch angle 15°

VIV is completely absent with the introduction of LR. Significantly, the maximum  $A^*$  value without the LR reaches up to 1, but introducing the LR reduces the  $A^*$  value to 0.8. These results were further confirmed from

Fig.17.b, by the  $F^*$  and  $F_v^*$  values, where  $F_v^*$  is almost varying linearly with the  $F^*$ , which is similar to the pitch angle 0° case. Thus, introducing the leading-edge rod, the VIV is greatly suppressed, but since the VAWT acquires energy from the incoming wind and runs faster, galloping instability is an unavoidable scenario in the VAWT shaft vibration system.

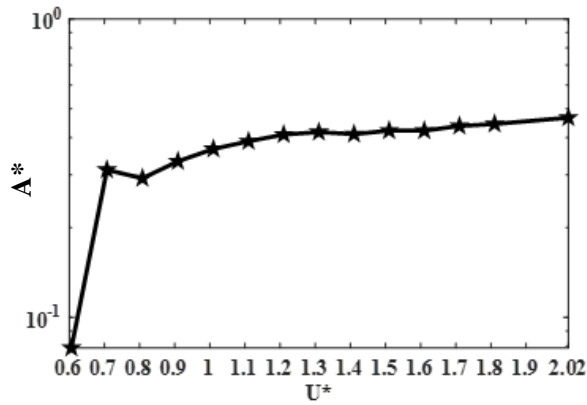
### 3.10 Wind Turbine Rotor Dynamics for LR at 21° Pitch Angle

Figure 18a illustrates the first transition. Following that,  $A^*=A/D$  displays a quasi-linear dependence with  $U^*$ , similar to the galloping type. As a result, with the introduction of LR, the VIV is non-existent similar to the previous study. Notably, the highest  $A^*$  value without the LR can reach up to 1.5, but the  $A^*$  value drops to 0.45 when the LR is introduced. The  $F^*$  and  $F_v^*$  data from Fig.18b, further supported these findings, showing that  $F_v^*$  practically varied linearly with  $F^*$ , much like in the galloping instance. The VIV is significantly reduced by introducing the leading-edge rod, and galloping stability dominates the vibration spectra as in the 15° LR study.

## 4. Conclusion

The D-VAWT has been designed and tested at wind speeds ranging from ( $U^* = 0.6$  to 2) for various pitch angles (0° to 21° by a step of 3°) and turbine tip speeds. The D-VAWT can oscillate both along and across wind directions, and the along wind direction acceleration data have been taken. The cylinder position and oscillating amplitude are directly related, according to the rotation law. Hence in this study, the FIV was identified based on the cylinder's displacement. The result outcomes are:

1. In the scenario where the pitch angle 0° is proportionate to the oscillating displacement ( $\alpha=rly$ ), the relationship between  $U^*$  and  $A^*$  is quasi-linear. This indicates the absence of a synchronization region and verifies the VIV's absence.



**Fig. 18a** Logarithmic Non-dimensional amplitude oscillations as a function of the reduced velocity for the pitch angle  $21^\circ$

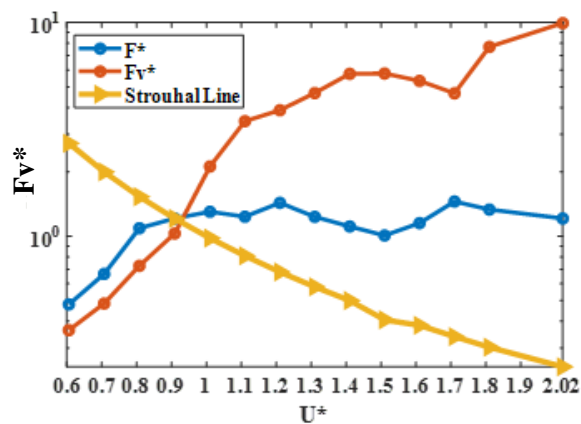


**Fig. 18b**  $F^*$  Normalized oscillation frequency;  $F_{v^*}$  Normalized vortex emission frequency; Strouhal Line as a function of decreased velocity for the value =  $0^\circ$  -  $45^\circ$  at pitch angle  $21^\circ$

Consequently, these fluid force types typically resemble the galloping kind of instability caused by motion. The relationship between oscillating frequency ( $F^*$ ) and vortex frequency ( $F_{v^*}$ ) deviates at a particular frequency spectrum at  $U^*=0.9$ . Hence as a confirmation, in the case of pitch angle  $0^\circ$ , there is no connection between the spectra, ensures galloping type FIV prevails.

2. Regarding the case for pitch angle  $3^\circ$ , the amplitude initially increases and remains constant in the range of  $0.6 < U^* < 1.01$ , and for the range ( $U^* = 1.1$  and  $1.2$ ), the value decreases considerably and started to increase when  $U^* = 1.3$  to  $2.02$ . The turbine rotor system experiences an increase and decrease in amplitude, that denotes the flow-induced vibration, could be VIV ( $0.6 < U^* < 1.2$ ) and galloping in the region ( $U^*=1.3$  to  $2.02$ ). Further confirmation happens when, the initial excitation frequency at ( $U^*=0.6$ ) drops dramatically from its natural frequency value of '1'. As  $U^*$  increases, so does  $F^*$ , until it reaches a value closer to '1', at which point it remains constant ( $U^*=0.8$ ) while the rotor oscillates considerably. At  $U^*=1.2$ , the synchronization region between the vortex shedding ( $F_{v^*}$ ) and oscillating frequency ( $F^*$ ) ends, at which the value of  $A^*$  practically is '0'. The region ( $0.9 < U^* < 1.2$ ) the

value of  $F^*$  and  $F_{v^*}$  are almost closer to the Strouhal line, which is the vortex emission frequency at rest, which suggests VIV. Further at  $1.3 < U^* < 2.02$ ,  $F_{v^*}$  value increases linearly and when  $U^* = 1.3$  to  $2.02$  the  $F_{v^*}$  is independent which moves farther from  $F^*$  which confirms there is no synchronization between the frequencies. Clearly these region experiences negative oscillations which confirms the presence of galloping.

3. Similar to the case of pitch angle  $3^\circ$  for  $6^\circ$ ,  $U^* = 0.6$  to  $1.4$  the region is in synchronization and VIV dominates the FIV. Between  $U^*= 1.4$  to  $2.02$  the region exhibits galloping due to high tip speed of the turbine.
4. For the scenario of pitch angle  $9^\circ$ , VIV is responsible for the FIV, in this case desynchronization happens at  $U^*=1.5$ ; but the amplitude remains high at the regions  $U^*=1.5$  and  $1.6$  and slowly reaches the lower branch, which is due to the D-VAWT rotating in the same direction as the vortices being shed, while vortex emission and cylinder oscillations (till  $U^*=1.4$ ) are synchronized. As the circulation of these vortices increases, so does the amplitude of the vibration.
5. For the pitch angle  $12^\circ$ , the initial lower branch takes a long period and reaches the upper branch and comes down, which is classical VIV happening and galloping is completely absent.
6. For the pitch angles  $15^\circ$ ,  $18^\circ$  and  $21^\circ$ , the VIV predominates and galloping is absent. Since there is a larger period of synchronization in these pitch angles, an effort is taken to identify the behavior of VIV with the introduction of leading-edge rod.
7. With a leading-edge rod attached to the D-VAWT two cases were studied at pitch angles  $15^\circ$  and  $21^\circ$ ; where it is interesting to note that the VIV was completely suppressed. This leads to galloping. But the maximum amplitudes prevail at  $15^\circ$  and  $21^\circ$  were greatly reduced.

## ACKNOWLEDGEMENTS

This research was supported by the Science Engineering Research Board (SERB), Department of Science & Technology (DST), Government of India, File No: C.R.G./2021/005720.

## CONFLICT OF INTEREST

The author has no conflicts to disclose.

## AUTHORS CONTRIBUTION

**C. B. Maheshwaran:** Idea formulation, Analytical processing, Examination and testing, Data collection and organization, Draft preparation, Creation of figures and graphs, **E. Karthik Vel:** Software engineering, Data Analysis, **S. Nadaraja Pillai:** Research framework, Refining and proofreading, Resources, Supervision.

## REFERENCES

- Abdelkefi, A., Hajj, M. R., & Nayfeh, A. H. (2012). Power harvesting from transverse galloping of square cylinder. *Nonlinear Dynamics*, 70(2), 1355–1363. <https://doi.org/10.1007/s11071-012-0538-4>
- Al-Mdallal, Q. M. (2004). *Analysis and computation of the cross-flow past an oscillating cylinder with two degrees of freedom* [Doctoral Dissertation, Memorial University of Newfoundland].
- Bachant, P., & Wosnik, M. (2016). Effects of Reynolds number on the energy conversion and near-wake dynamics of a high solidity vertical-axis cross-flow turbine. *Energies*, 9(2), 73. <https://doi.org/10.3390/en9020073>
- Bel Mabrouk, I., ELHami, A., Walha, L., Zghal, B., & Haddar, M. (2017). Dynamic vibrations in wind energy systems: Application to vertical axis wind turbine. *Mechanical Systems and Signal Processing*, 85, 396–414. <https://doi.org/10.1016/j.ymsp.2016.08.034>
- Blackburn, H. M., Elston, J. R., & Sheridan, J. (1999). Bluff-body propulsion produced by combined rotary and translational oscillation. *Physics of Fluids*, 11(1), 4–6. <https://doi.org/10.1063/1.869912>
- Castellani, F., Astolfi, D., Bechetti, M., & Berno, F. (2018). Experimental and numerical analysis of the dynamical behavior of a small horizontal-axis wind turbine under unsteady conditions: Part I. *Machines*, 6(4). <https://doi.org/10.3390/machines6040052>
- Dunne, R., & McKeon, B. J. (2015). Dynamic stall on a pitching and surging airfoil. *Experiments in Fluids*, 56(8), 157. <https://doi.org/10.1007/s00348-015-2028-1>
- Elangovan, K., & Pillai, S. N. (2025). Effect of pitch angle on structural and aerodynamic characteristics of vertical-axis wind turbines (VAWTs) using leading-edge protuberance blades. *Energies*, 18(2), 286. <https://doi.org/10.3390/en18020286>
- Fatahian, E., Ismail, F., Ishak, M. H. H., & Chang, W. S. (2024). Novel passive flow control method using leading-edge prism-shaped cylinder: Performance enhancement of vertical-axis wind turbines. *Physics of Fluids*, 36(11). <https://doi.org/10.1063/5.0233464>
- Govardhan, R. N., & Williamson, C. H. K. (2006). Defining the ‘modified Griffin plot’ in vortex-induced vibration: revealing the effect of Reynolds number using controlled damping. *Journal of Fluid Mechanics*, 561, 147–180. <https://doi.org/10.1017/S0022112006000310>
- Hamdi, H., Mrad, C., Hamdi, A., & Nasri, R. (2014). Dynamic response of a horizontal axis wind turbine blade under aerodynamic, gravity and gyroscopic effects. *Applied Acoustics*, 86, 154–164. <https://doi.org/10.1016/j.apacoust.2014.04.017>
- Kaczinski, M. R., Dexter, R. J., & Van Dien, J. P. (1998). *Fatigue-resistant design of cantilevered signal, sign and light supports*. Nchrp: Vol. NCHRP Repo (p. 176).
- Karthik Vel, E., & Nadaraja Pillai, S. (2024). Vibration control of the straight bladed vertical axis wind turbine structure using the leading-edge protuberanced blades. *Engineering Structures*, 319, 118806. <https://doi.org/https://doi.org/10.1016/j.engstruct.2024.118806>
- Lu, L., Qin, J. M., Teng, B., & Li, Y. C. (2011). Numerical investigations of lift suppression by feedback rotary oscillation of circular cylinder at low Reynolds number. *Physics of Fluids*, 23. <https://doi.org/10.1063/1.3560379>
- Maheshwaran, C. B., Gopal, R., Chandrasekar, V. K., & Pillai, S. N. (2023). Chaotic vibration characteristics of Vertical Axis Wind Turbine (VAWT) shaft system. *Wind and Structures, An International Journal*, 36(3), 215–220. <https://doi.org/10.12989/was.2023.36.3.215>
- McLaren, K., Tullis, S., & Ziada, S. (2012). Measurement of high solidity vertical axis wind turbine aerodynamic loads under high vibration response conditions. *Journal of Fluids and Structures*, 32, 12–26. <https://doi.org/https://doi.org/10.1016/j.jfluidstructs.2012.01.001>
- Miller, M. A., Duvvuri, S., Brownstein, I., Lee, M., Dabiri, J. O., & Hultmark, M. (2018). Vertical-axis wind turbine experiments at full dynamic similarity. *Journal of Fluid Mechanics*, 844, 707–720. <https://doi.org/10.1017/jfm.2018.197>
- Mohamed, M. H. (2012). Performance investigation of H-rotor Darrieus turbine with new airfoil shapes. *Energy*, 47(1), 522–530. <https://doi.org/10.1016/j.energy.2012.08.044>
- Davandeh, N., & Maghrebi, M. J. (2023). Leading Edge Radius Effects on VAWT Performance. *Journal of Applied Fluid Mechanics*, 16(9). <https://doi.org/10.47176/jafm.16.09.1626>
- Nazarinia, M., Lo Jacono, D., Thompson, M. C., & Sheridan, J. (2009a). Flow behind a cylinder forced by a combination of oscillatory translational and rotational motions. *Physics of Fluids*, 21(5), 51701. <https://doi.org/10.1063/1.3139184>
- Nazarinia, M., Lo Jacono, D., Thompson, M. C., & Sheridan, J. (2009b). The three-dimensional wake of a cylinder undergoing a combination of translational and rotational oscillation in a quiescent fluid. *Physics of Fluids*, 21(6), 64101. <https://doi.org/10.1063/1.3147935>
- Nguyen, M. T., Balduzzi, F., & Goude, A. (2021). Effect of pitch angle on power and hydrodynamics of a vertical axis turbine. *Ocean Engineering*, 238, 109335. <https://doi.org/https://doi.org/10.1016/j.oceaneng.2021.109335>

- Peng, Y. X., Xu, Y. L., Zhan, S., & Shum, K. M. (2019). High-solidity straight-bladed vertical axis wind turbine: Aerodynamic force measurements. *Journal of Wind Engineering and Industrial Aerodynamics*, *184*, 34–48. <https://doi.org/10.1016/j.jweia.2018.11.005>
- Piersol, A. G., & Paez, T. L. (Eds.). (2010). *Harris' Shock and Vibration Handbook* (6th Editio). McGraw-Hill Education.
- Ross, H., & Polagye, B. (2022). Effects of dimensionless parameters on the performance of a cross-flow current turbine. *Journal of Fluids and Structures*, *114*, 103726. <https://doi.org/https://doi.org/10.1016/j.jfluidstructs.2022.103726>
- Simão Ferreira, C. J., Bijl, H., Van Bussel, G., & Van Kuik, G. (2007). Simulating dynamic stall in a 2D VAWT: Modeling strategy, verification and validation with particle image velocimetry data. *Journal of Physics: Conference Series*, *75*(1). <https://doi.org/10.1088/1742-6596/75/1/012023>
- Singh, S. P., & Mittal, S. (2005). Flow past a cylinder: Shear layer instability and drag crisis. *International Journal for Numerical Methods in Fluids*, *47*(1), 75–98. <https://doi.org/10.1002/fld.807>
- Vicente-Ludlam, D., Barrero-Gil, A., & Velazquez, A. (2017). Flow-Induced Vibration of a rotating circular cylinder using position and velocity feedback. *Journal of Fluids and Structures*, *72*, 127–151. <https://doi.org/https://doi.org/10.1016/j.jfluidstructs.2017.05.001>
- Wei, S., Zhao, J. S., Han, Q., & Chu, F. (2015). Dynamic response analysis on torsional vibrations of wind turbine geared transmission system with uncertainty. *Renewable Energy*, *78*. <https://doi.org/10.1016/j.renene.2014.12.062>
- Zhong, J., Li, J., Guo, P., & Wang, Y. (2019). Dynamic stall control on a vertical axis wind turbine aerofoil using leading-edge rod. *Energy*, *174*, 246–260. <https://doi.org/10.1016/j.energy.2019.02.176>
- Zuo, D., & Letchford, C. (2010). Wind-induced vibration of a traffic-signal-support structure with cantilevered tapered circular mast arm. *Engineering Structures*, *32*, 3171–3179. <https://doi.org/10.1016/j.engstruct.2010.06.005>